INTERNATIONAL JOURNAL FOR NUMERICAL METHODS IN FLUIDS
Int. J. Numer. Meth. Fluids 2010; **63**:681–700
Published online 23 June 2009 in Wiley InterScience (www.interscience.wiley.com). DOI: 10.1002/fld.2106

Prediction of entrance length and mass suction rate for a cylindrical sucking funnel

Dipti Prasad Mishra and Sukanta K. Dash*, †

Department of Mechanical Engineering, IIT, Kharagpur 721 302, India

SUMMARY

Conservation equations for mass, momentum and energy have been solved numerically for a cylindrical funnel with louvers (lateral openings on the side wall of the cylindrical funnel through which air can come into it) to compute the suction rate of air into the funnel. The nozzle placed centrally at the bottom of the cylinder ejects high-velocity hot gaseous products so that atmospheric air gets sucked into the funnel. The objective of the work is to compute the ratio of the rate of mass suction to that of the mass ejected by the nozzle for different operating conditions and geometrical size of the funnel. From the computation it has been found that there exists optimum funnel diameter and optimum funnel height for which the mass suction is the highest. The protruding length of the nozzle into the funnel has almost no effect on the mass suction rate after a certain funnel height. The louvers opening area has a very high impact on the mass suction rate. The entrance length for such a sucking funnel is strikingly much lower compared with a simple cylindrical pipe having uniform flow at the inlet at same Reynolds number. A new correlation has been developed to propose the entrance length for a sucking pipe, the rate of mass suction into it and the exhaust plume temperature over a wide range of operating parameters that are normally encountered in a general funnel operations of naval or merchant ship. Copyright © 2009 John Wiley & Sons, Ltd.

Received 16 January 2009; Revised 7 May 2009; Accepted 16 May 2009

KEY WORDS: funnel; louvers; suction; nozzle; entrance length; ship

INTRODUCTION

The funnels of naval or merchant ship receive the hot combustion products from a nozzle that is placed at the center of the funnel at its bottom. The high-velocity gas coming out of the nozzle creates suction inside the funnel for which the atmospheric air gets sucked into the funnel, thereby reducing the temperature of the flue gas to a great extent which is desired for the naval ship operation. In order to bring down the temperature of the flue gas to a much lower level (because the enemy's ship cannot detect it in mid sea), it is required to design the funnel in such a way that it can suck the highest amount of air. Hence, the geometrical size of the funnel plays a role in

*Correspondence to: Sukanta K. Dash, Department of Mechanical Engineering, IIT, Kharagpur 721 302, India.
†E-mail: sdash@mech.iitkgp.ernet.in

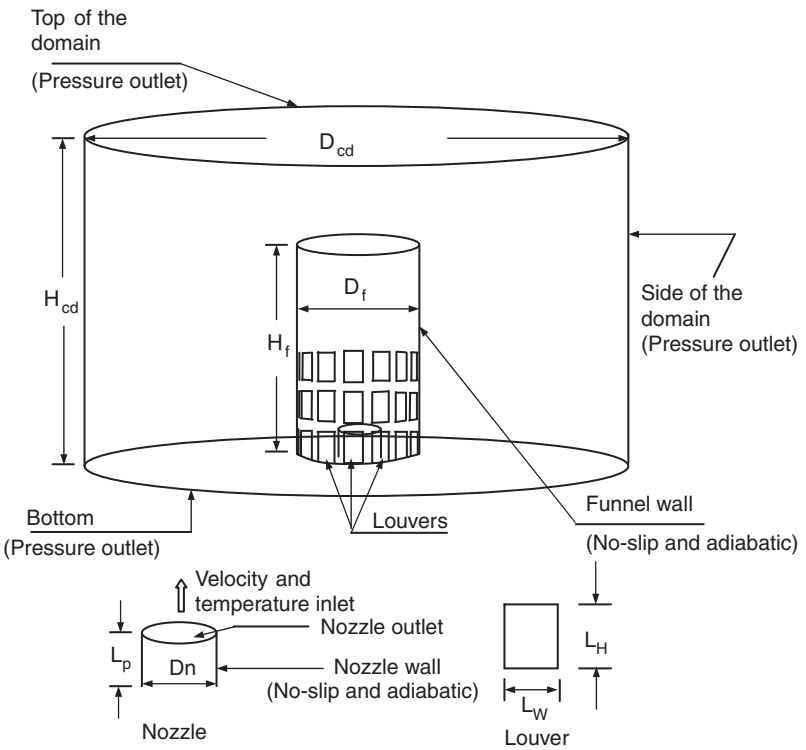

Figure 1. Schematic diagram of computational domain with the cylindrical funnel and a pictorial view of boundary conditions applied to it.

deciding it. The main objective of the present work is to determine the ratio of mass suction to the mass injected as a function of different geometrical and operating parameters. While computing the flow field in the funnel as well as outside it to find the mass ingress of air into it we could compute the entrance length of the flow inside the funnel. The computation of the entrance length is done by just plotting the centerline velocity against the height of the funnel. The onset of invariance of the velocity with the funnel height is the indication of the establishment of entrance length. A general correlation for the entrance length has been obtained from the CFD analysis as a function of different pertinent input parameters varying over a wide range of operating conditions for a sucking cylindrical funnel.

MATHEMATICAL FORMULATION

The computational investigation is carried out for a cylindrical funnel (of diameter, D_f and height, H_f as shown in Figure 1). The funnel is closed at the bottom and opened at the top to the surrounding atmosphere. At the bottom of the funnel a nozzle of diameter, D_n having a protrusion length of L_p (into the funnel) is placed at the center to supply high-velocity air jet. Another cylindrical computational domain of diameter, D_{cd}, (10 times of D_f) and height, H_{cd} (2 to 3 times

DOI: 10.1002/fld

of H_f) is placed around the funnel so that the boundary condition can be applied on the boundary of the computational domain for suction to take place near the louvers cut on the funnel. The louvers are kept rectangular in shape ($L_H = 0.8\,\text{m}$ and $L_w = 0.6\,\text{m}$, 12 louvers on one stack and there are a maximum of four stacks used depending on the values of A_L. Distance between the stacks was 0.5 m). The flow field in the domain would be computed by using three dimensional, incompressible Navier–Stokes equations with a two equation k–ε turbulence model along with the energy equation. The fluid used in the simulation is air, at temperatures of 300–700 K, and is treated to be incompressible at the injection velocity (which is below 100 m/s).

GOVERNING EQUATIONS

The governing equations for the above analysis can be written as:

Continuity:

$$\nabla \cdot (\rho \mathbf{v}) = 0 \tag{1}$$

Momentum:

$$\nabla \cdot (\rho \mathbf{v}\mathbf{v}) = -\nabla p + \nabla \cdot (\bar{\bar{\tau}}) - (\rho_\infty - \rho) g \tag{2}$$

The density ρ is taken to be a function of temperature according to ideal gas law, while laminar viscosity μ and thermal conductivity are kept constant. Extensive numerical study has shown that the mass suction into the funnel is an extremely weak function of μ and does not depend on thermal conductivity. The Boussinesq approximation is not adopted in the model since the variation of ρ with temperature is tremendous in the range of operating parameters.

Energy:

$$\frac{D(\rho T)}{Dt} = \frac{\partial}{\partial x_i}\left[\left(\frac{\mu}{Pr} + \frac{\mu_t}{Pr_t}\right)\frac{\partial T}{\partial x_i}\right] \tag{3}$$

The stress tensor $\bar{\bar{\tau}}$ is given by

$$\bar{\bar{\tau}} = \mu^{\text{eff}}(\nabla \mathbf{v} + \nabla \mathbf{v}^{\text{T}}) \tag{4}$$

effective viscosity $\mu^{\text{eff}} = (\mu + \mu_t)$

Turbulence kinetic energy—k:

$$\nabla \cdot (\rho \mathbf{v} k) = \nabla \cdot \left(\frac{\mu_t}{\sigma_k}\nabla k\right) + G_k - \rho\varepsilon \tag{5}$$

Rate of dissipation of k:

$$\nabla \cdot (\rho \mathbf{v} \varepsilon) = \nabla \cdot \left(\frac{\mu_t}{\sigma_\varepsilon}\nabla \varepsilon\right) + \frac{\varepsilon}{k}(C_{1\varepsilon} G_k - C_{2\varepsilon}\rho\varepsilon) \tag{6}$$

The turbulent viscosity μ_t is computed from

$$\mu_t = \rho C_\mu \frac{k^2}{\varepsilon} \tag{7}$$

DOI: 10.1002/fld

The term G_k representing the production of turbulent kinetic energy is computed from

$$G_k = \mu_t(\nabla \mathbf{v} + (\nabla \mathbf{v})^{\mathrm{T}}) : \nabla \mathbf{v} \tag{8}$$

σ_k and σ_ε are the Prandtl numbers for k and ε.

The constants used in the above k–ε equations are the following, although these constants are normally used for internal flow but for the present case we have not changed the constants (there is a provision in Fluent to change the constants).

$$C_{1\varepsilon} = 1.44, \quad C_{2\varepsilon} = 1.92, \quad C_\mu = 0.09, \quad \sigma_k = 1.0, \quad \sigma_\varepsilon = 1.3, \quad Pr_t = 1$$

BOUNDARY CONDITIONS

The boundary conditions can be seen from Figure 1 pictorially. The funnel wall and nozzle wall are solid and have been given a no-slip boundary condition. Pressure outlet boundary conditions have been imposed at the outer periphery, at the top surface and at the bottom of the annular computational domain and velocity inlet boundary condition has been employed at the nozzle outlet which supplies high-velocity air in to the funnel.

At the pressure outlet boundary, the velocity will be computed from the local pressure field so as to satisfy the continuity, but all other scalar variables such as T, k and ε are computed from the zero gradient condition, Dash [1].

The turbulent quantities, k and ε, on the first near wall cell have been set from the equilibrium log law wall function as has been described by Jha and Dash *et al.* [2–4]. The turbulent intensity at the inlet of the nozzle has been set to 2% with the inlet velocity being known and the back flow turbulent intensity at all the pressure outlet boundaries has been set to 5%. If there is no back flow at a pressure outlet boundary then the values of k and ε are computed from the zero gradient condition at that location.

NUMERICAL SOLUTION PROCEDURE

Three-dimensional equations of mass, momentum, energy and turbulence have been integrated over the control volume and the subsequent equations have been discretized over the control volume using the finite volume technique to yield a set of algebraic equations that could be solved by the algebraic multi grid solver of **Fluent 6.3** in an iterative manner by imposing the above boundary conditions. First-order upwind scheme (for convective variables) was considered for momentum as well as for the turbulent discretized equations. After a first-hand converged solution could be obtained the scheme was changed over to the second-order upwind so as to get little better accuracy. However, before switching to the higher-order scheme the meshes near the funnel wall and inside the funnel area were refined to half of its original size. This will increase the number of meshes significantly and hence the computational time. Thus, a careful mesh description is needed from the beginning so that adoption to finer meshes for higher-order computing should not be prohibitively large. A preliminary mesh on the louvers and on the funnel wall as well as in the

DOI: 10.1002/fld

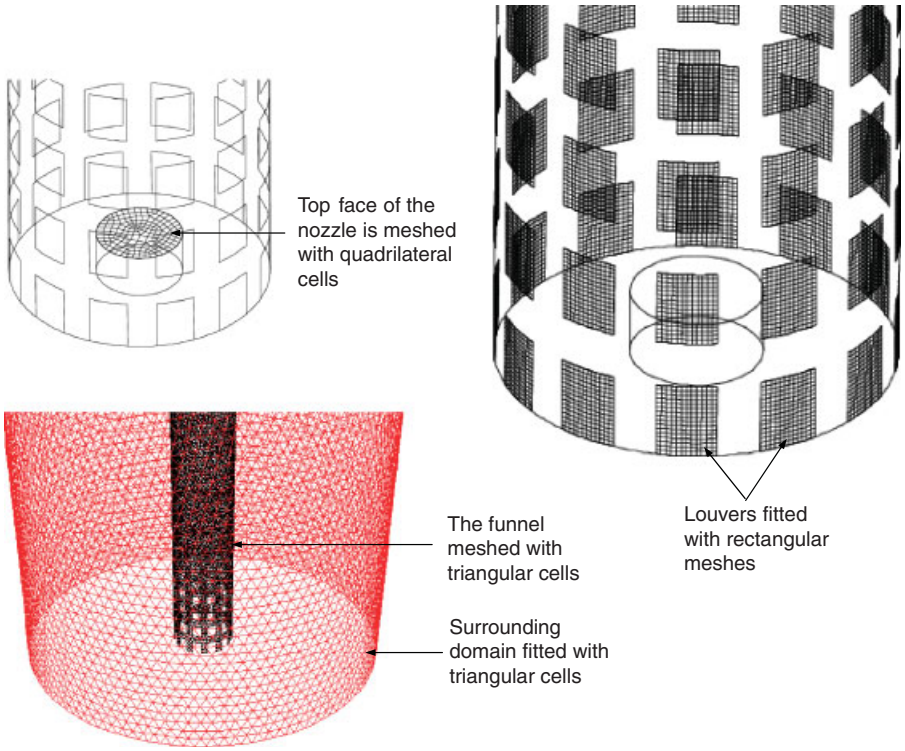

Figure 2. Cutaway view of the meshes in and around the louvers.

computational domain can be seen from Figure 2. We used about 210 000 cells at the beginning where first-order upwinding scheme could converge and later on after adoption the cells could grow to 760 000 and first-order upwinding solutions still could give a better converged solution with a maximum change of only 3% in the mass suction rate. Then we adopted the second-order scheme and continued the computation which still took some more iterations to converge and the mass suction rate could change only in the range of 0.25–0.5% where we stopped the computation.

The rectangular louvers were fitted with the rectangular face meshes (12×16) and the surrounding area (inside the funnel as well as outside) was fitted with triangular cells due to complexity of the geometry which can be seen from Figure 2. The funnel top and the outside cylindrical curved surfaces were meshed with quadrilateral cells.

SIMPLE algorithm with a PRESTO scheme for the pressure velocity coupling was used for the pressure correction equation. Under relaxation factors of 0.3 for pressure, 0.7 for momentum and 0.5 for k and ε and 1 for temperature were used for the convergence of all the variables. Tetrahedral cells were used for the entire computational domain because it was the only choice in such a complicated geometry. The top surface of the funnel and the nozzle inlet was paved with quadrilateral cells for better mesh control. Convergence of the discretized equations was said to have been achieved when the whole field residual for all the variables fell below 10^{-3} for u, v, w, p, k and ε, whereas for energy the residual level was kept at 10^{-6}.

DOI: 10.1002/fld

RESULTS AND DISCUSSIONS

Matching with other computations

We tried to match the mass suction into a confined jet in a cylindrical funnel where suction was only allowed at the bottom opening of the funnel just close to the nozzle as shown in Figure 3(a). Figure 3(a) also shows the grid arrangement that was used to compute the mass suction. A comparison between $Q_{\text{suc}}/Q_{\text{inlet}}$ with that of the experiment of Singh *et al.* [5] and Pritchard's relation for the confined jet can be seen from Figure 3(a). The present CFD result matches well with the analytical solution developed by Pritchard *et al.* [6] and also reasonably well with that of the experiment.

An experimental observation

Before proceeding to the mass entrainment computation for the actual funnel we did a simulation for the experimental setup which we had in our laboratory. The experimental setup was a small scale model ($H_{\text{f}}=1.2\,\text{m}$, $D_{\text{f}}=0.14\,\text{m}$, $D_{\text{n}}=0.019\,\text{m}$ with $A_{\text{L}}=0.0232\,\text{m}^2$) (Figure 3(b)) where the velocity could be measured at the outlet of the funnel by a hot wire anemometer from which the mass ingress could be computed after subtracting the known flow to the nozzle. The flow to the nozzle was measured by a rotameter and the experiment was done at room temperature. The mass entrainment into the funnel varies linearly with that of the mass flow rate from the nozzle for low $Re(<8000)$. For this reason the ratio of mass ingress to the mass injected remains almost flat at low Re. The present CFD computation shows a good degree of matching with the experimental observation as can be seen from Figure 4. Figure 4 also shows a diagram where the entrance length ($L_{\text{e}}=L-H_{\text{L}}$) can be seen in the funnel. At about 0.9 m from the bottom of the funnel the velocity profile seems to have developed fully, whereas at 0.5 and 0.7 m the flow field has not been developed. We will compute this for the actual funnel (used in the ship) for many different parameters.

The experimental uncertainty in the mass suction rate has been shown in Figure 4. In this particular context the sources of errors in the experimental measurements are the measurement of length by scale, velocity measurement by anemometer and inlet flow measurement by the rotameter. For the computation of mass suction rate the value of density was taken at room temperature of 20°C and at a pressure of 101 kPa. The errors in the laboratory temperature and pressure readings will affect the value of density which is also taken into consideration in the uncertainty analysis in Appendix A. The details of the computation of uncertainty for a particular case have been presented in Appendix A. From the figure it is clear that the uncertainty in the measurement process is limited within 2–2.6%.

Effect of Re_{n} on ratio of rate of mass ingress to the rate of mass injected from the nozzle

Figure 5 shows the value of $\dot{m}_{\text{suc}}/\dot{m}_{\text{inl}}$ as a function of Re_{n}, where the nozzle fluid temperature varies from 300 K to 723 K. It can be seen from the plot that the ratio of mass suction to the mass inlet slowly rises with Re_{n} unlike the case for the experiment where the ratio was almost constant. If the inlet mass flow increases the mass entrainment also increases, but very slowly at high Re_{n} for which the ratio very slowly increases with Re_{n} at a constant temperature. But as the temperature of the nozzle fluid increases the mass entrainment increases rapidly at a constant Re_{n} because the plume becomes too buoyant. A correlation from the present CFD computation

DOI: 10.1002/fld

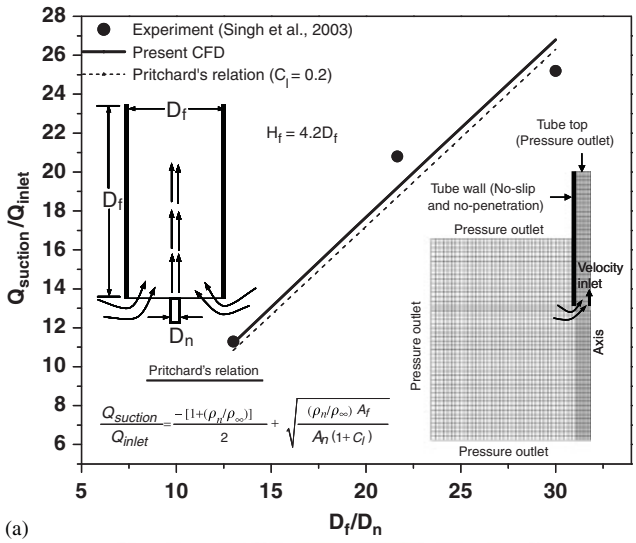

(a)

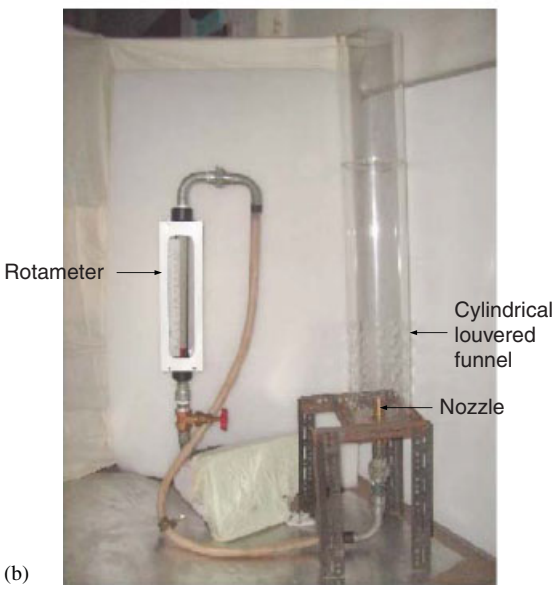

(b)

Figure 3. (a) Entrainment ratio as a function of D_f/D_n for a wall constrained jet: A comparison among the experiment, present CFD and Pritchard's relation and (b) snapshot of experimental setup.

has been developed to predict the ratio of rate of mass ingress to that of inlet mass flow rate as per Equations (9) and (10) out of 228 numerical experiments

$$\frac{\dot{m}_{\mathrm{suc}}}{\dot{m}_{\mathrm{inl}}}=(2.845+0.0258\ln(Re_{\mathrm{n}}))\left(\frac{A_{\mathrm{L}}}{D_{\mathrm{n}}^2}\right)^{0.3512}\left(-0.33+0.282\frac{D_{\mathrm{f}}}{D_{\mathrm{n}}}-0.031\left(\frac{D_{\mathrm{f}}}{D_{\mathrm{n}}}\right)^2\right)\left(\frac{T_{\mathrm{n}}}{T_{\infty}}\right)^{0.569} \quad (9)$$

DOI: 10.1002/fld

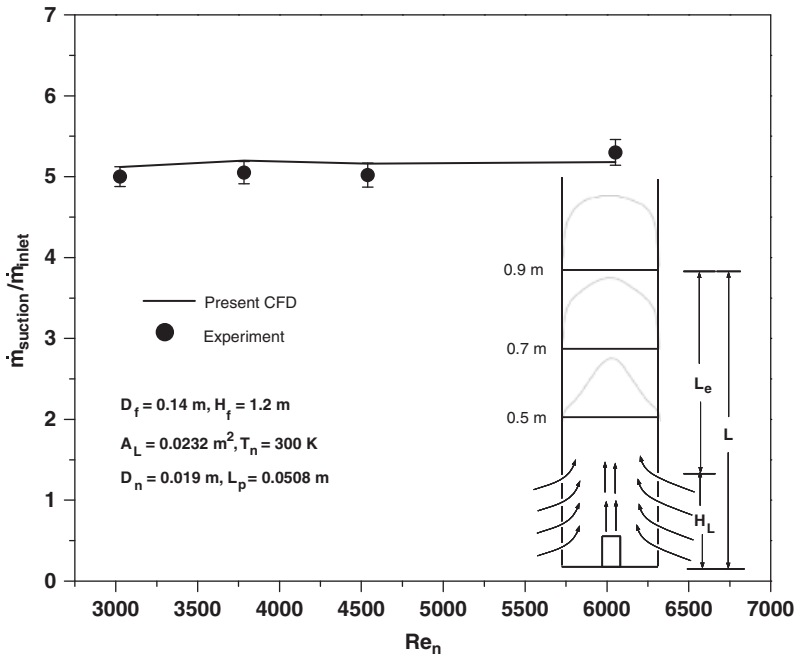

Figure 4. A comparison between the computational and experimental result (with uncertainty) for ratio of mass entrained to mass injected as a function of Re_n.

$$\frac{\dot{m}_{suc}}{\dot{m}_{inl}} = (1.273 + 0.01\ln(Re_n))\left(\frac{A_L}{D_n^2}\right)^{0.829}\left(0.144 + 0.007\frac{D_f}{D_n} - 0.00074\left(\frac{D_f}{D_n}\right)^2\right)\left(\frac{T_n}{T_\infty}\right)^{0.7374} \quad (10)$$

over the range of parameters such as $Re_n = 10^4$–10^8, $D_f/D_n = 2.2$–4.55, $A_L/D_n^2 = 3$–13.22 and $T_n/T_\infty = 1$–2.41 for Equation (9). For Equation (10) the range of parameters is $Re_n = 10^4$–10^8, $D_f/D_n = 4.6$–9.1, $A_L/D_n^2 = 13.22$–55 and $T_n/T_\infty = 1$–2.41. Figure 5 also shows a comparison between direct CFD result and the result from the correlation equation (9). There seems to be a good agreement between the correlation and the CFD result. The correlation equation (9) has a maximum error (CFD as the base) of 9.0% only at two points at low Re_n and rest 108 data points are in the range of 7% error which is pretty well acceptable for any engineering calculation.

Effect of Re_n on exhaust plume temperature

A correlation has been developed to predict T_f/T_∞ (ratio of funnel exit gas temperature to that of surroundings temperature) from 132 numerical computations as follows:

$$\frac{T_f}{T_\infty} = (2.256 + 0.01084\ln(Re_n))\left(\frac{A_L}{D_n^2}\right)^{1.119}\left(0.0554 - 0.0084\frac{D_f}{D_n} + 0.00042\left(\frac{D_f}{D_n}\right)^2\right) \times \left(\frac{T_n}{T_\infty}\right)^{0.7087}\left(\frac{\dot{m}_{suc}}{\dot{m}_{inl}}\right)^{-0.6448} \quad (11)$$

DOI: 10.1002/fld

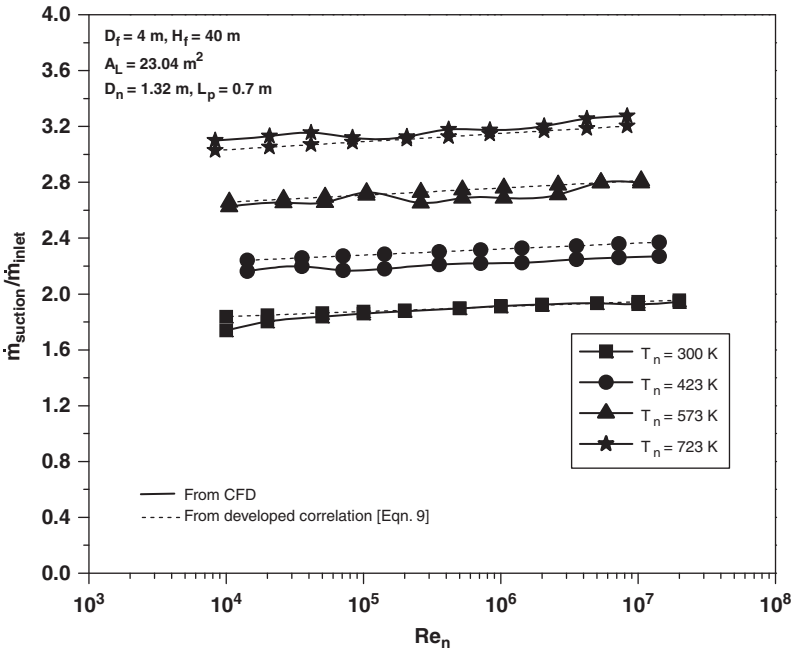

Figure 5. Ratio of rate of mass suction to the rate of inlet mass flow as a function of Re_n and nozzle fluid temperature: A comparison with the developed correlation.

The range parameters for Equation (11) are $Re_n = 4 \times 10^3$–10^8, $D_f/D_n = 3.03$–9.1, $A_L/D_n^2 = 13.22$–55.1 and $T_n/T_\infty = 1.4$–2.41. It should be noted that the value of $\dot{m}_{suc}/\dot{m}_{inl}$ will be determined either from Equations (9) or (10) depending upon the range of D_f/D_n and A_L/D_n^2. A comparison between CFD computed temperature and Equation (11) has been shown in Figure 6. There seems to be a good agreement between the developed correlation and the computed results (maximum error being limited to only 2%).

Effect of D_f/D_n on ratio of rate of mass ingress to the rate of mass injected from the nozzle

Figure 7 shows the effect of D_f/D_n on $\dot{m}_{suc}/\dot{m}_{inl}$ for different nozzle fluid temperature. At $D_f/D_n = 4.55$ highest mass suction occurs into the funnel for all the nozzle fluid temperature considered in the range of 300–573 K. As D_f/D_n becomes more than 4.55 the mass suction rate into the funnel again decreases. This means that this is the optimum ratio for the geometry where mass flow rate into the funnel can be highest. The high-velocity jet coming from the nozzle into the funnel creates a low pressure little away from the nozzle tip and then the pressure slowly recovers toward the funnel top where it becomes equal to the atmospheric pressure. Owing to this the atmospheric air from outside the funnel gets sucked into the funnel. If the funnel diameter is too high then the louvers placed on the funnel wall are too away from the zone of low pressure and across the louvers the pressure differential is too less for which the mass suction becomes less for higher diameter funnel. As the funnel diameter decreases then the pressure differential across the louvers increases and the mass suction into the funnel increases. But if the funnel diameter decreases too much, then it offers a lot of viscous resistance to the flow of air inside it for

DOI: 10.1002/fld

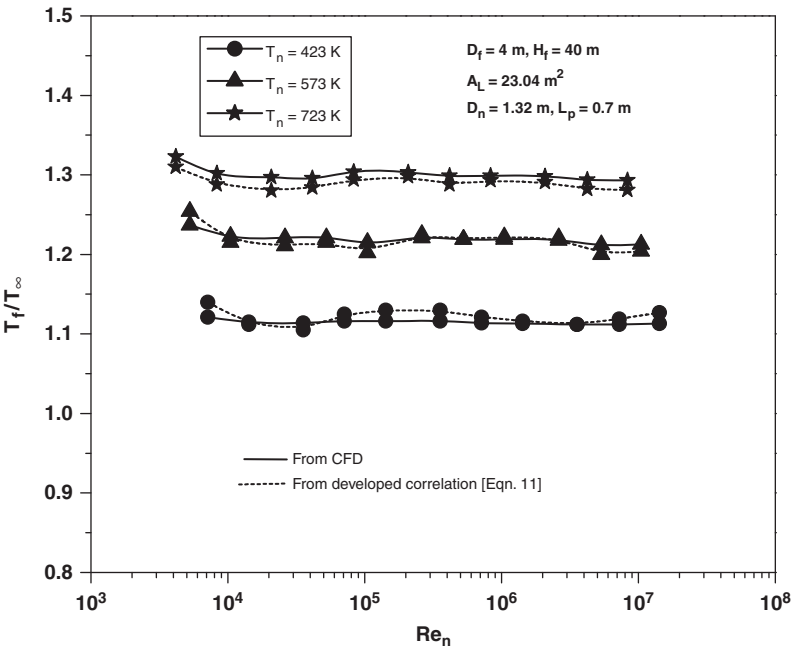

Figure 6. The funnel outlet temperature as a function of Re_n and nozzle fluid temperature: A comparison with the developed correlation.

which the mass suction again falls. Thus this is the reason for having an optimum funnel diameter where mass suction can be the highest. D_f/D_n has the significant effect on the mass suction rate. The mass suction rate can change by 130% if D_f/D_n changes from 2.2 to 4.55. Figure 7 also shows a comparison with the developed correlation which looks also very nice. There are two correlations developed for two ranges of D_f/D_n, Equation (9) is for the range $2.2 \leqslant D_f/D_n \leqslant 4.55$ and Equation (10) is for the range $4.6 \leqslant D_f/D_n \leqslant 9.1$. This has to be done to have a better fit for the curves and to keep the relative errors much less below 10%. Equation (10) has been developed from 118 data points and only 2 data points show errors to the level of 10% and all other data points show errors much less than 7%.

Effect of funnel diameter and size of louvers on centerline pressure

Figure 8 shows the centerline pressure of the funnel as a function of funnel diameter. It can be seen that when the diameter is 4 m the pressure at the nozzle exit is 175 Pa and when the diameter is 6 m then the static pressure falls to 50 Pa and again the pressure rises to 150 Pa when the diameter rises to 9 m. At a funnel diameter of 6 m there is the highest mass suction into the funnel. Normally, the pressure at the exit of the nozzle is regarded as a back pressure. When the number of louvers was varied from 48 to 96 on a 4 m diameter funnel (keeping the louvers area same) the centerline pressure hardly changed in its shape and value which can be seen from Figure 9. Thus it can be told that by making the louvers half in terms of its area the pressure at the nozzle exit was unaffected as well as the mass suction into the funnel (Figure 10). Thus the size of the louvers has to be made very small in order to see a change in the nozzle exit pressure which was not done in

DOI: 10.1002/fld

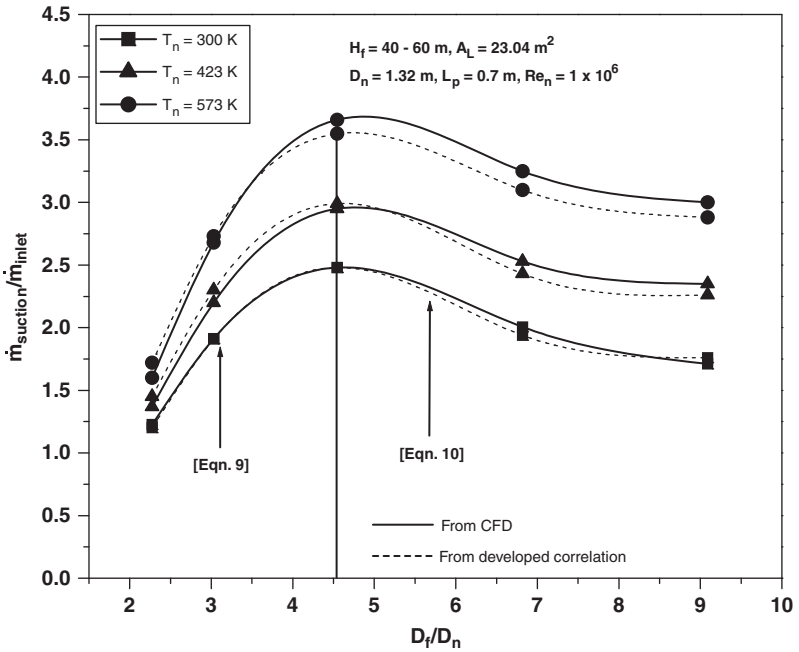

Figure 7. Ratio of rate of suction to the rate of inlet mass flow as a function of D_f/D_n and nozzle fluid temperature: A comparison with the developed correlation.

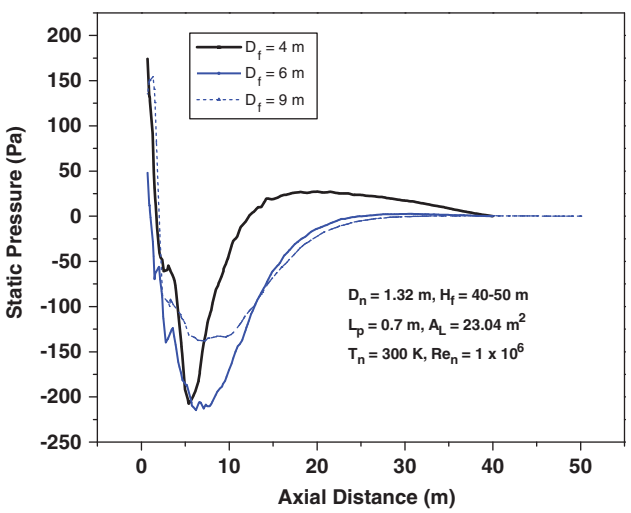

Figure 8. Centerline pressure as a function of diameter of the funnel.

DOI: 10.1002/fld

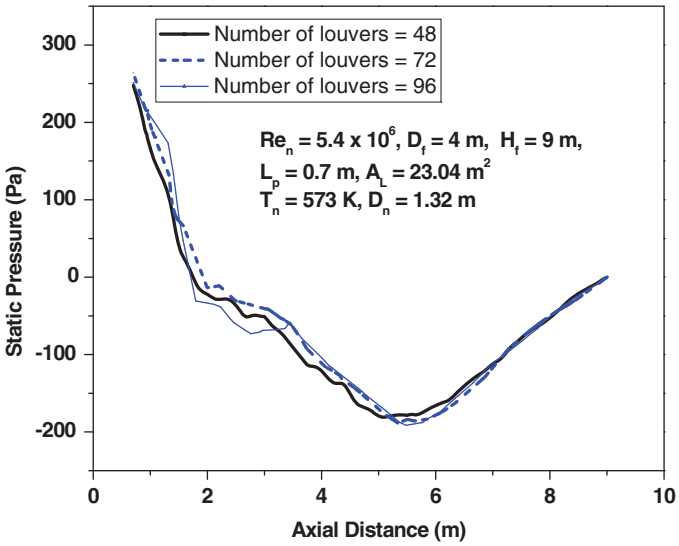

Figure 9. Centerline pressure as a function of louvers number of the funnel.

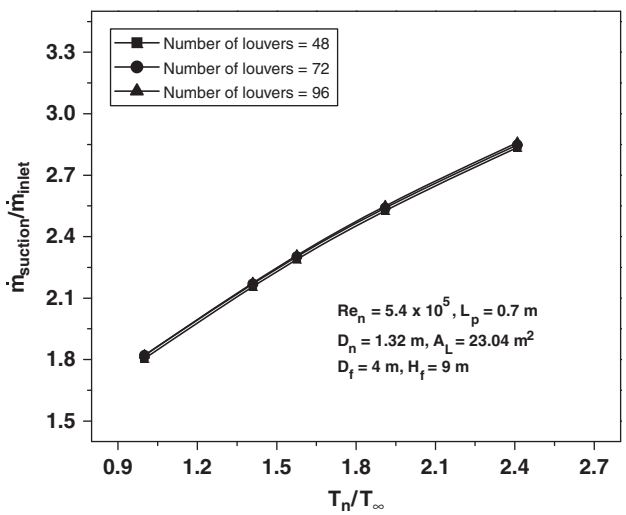

Figure 10. Ratio of rate of mass suction to the rate of inlet mass flow as a function of louvers number (for a constant louvers opening area of 23.04 m^2).

the present study because this will involve too many meshes and simulation difficulties. Moreover, the present geometrical simulation is probably not suitable to study back pressure effect on the engine due to changes in louvers area or its size.

DOI: 10.1002/fld

Effect of A_L/D_n^2 on ratio of rate of mass ingress to the rate of mass injected from the nozzle

Figure 11 shows the effect of A_L/D_n^2 on the mass suction rate into the funnel. As A_L/D_n^2 increases the mass suction into the funnel increases. After the parameter D_f/D_n the second most significant parameter influencing the mass suction rate is A_L/D_n^2. By making a change of A_L/D_n^2 from 2.2 to 13 the mass suction rate can be changed by 90%. The louvers opening area allows the outside mass to come into the funnel, so a rise in it will cause a rise in the mass suction. But after a certain value of the opening area the mass suction will not rise much, rather will attain a constant value. This can happen quickly for a short funnel and for a long funnel it will take a larger value of opening area to attain a constant suction rate. The particular case shown in Figure 11 depicts that after a value of $A_L/D_n^2 = 14$ the mass suction rate could be constant. In the computation we have made change to the size of the louvers, the louvers opening area was changed by simply adding more louvers symmetrically into the funnel. As has been discussed in the last section, the effect of size of the louvers on the mass suction is virtually nothing, unless they are too tiny and large in numbers. This particular effect has not been studied in the present work. The developed correlation is also plotted on the CFD prediction in Figure 11, which gives a good impression that the developed correlation can be used in practice.

Effect of A_L/D_n^2 on exhaust plume temperature

A correlation has been developed from 165 numerical simulations to predict T_f/T_∞ for the range of parameters given as $Re_n = 10^4$–10^8, $D_f/D_n = 2.2$–3.03, $A_L/D_n^2 = 3$–13.2 and $T_n/T_\infty = 1.4$–2.41.

$$\frac{T_f}{T_\infty} = (5.295 + 0.002\ln(Re_n))\left(\frac{A_L}{D_n^2}\right)^{0.02}\left(0.106 + 0.0555\frac{D_f}{D_n} - 0.0087\left(\frac{D_f}{D_n}\right)^2\right) \times \left(\frac{T_n}{T_\infty}\right)^{0.469}\left(\frac{\dot{m}_{suc}}{\dot{m}_{inl}}\right)^{-0.193} \quad (12)$$

The value of $\dot{m}_{suc}/\dot{m}_{inl}$ has to be determined from Equation (9). Figure 12 shows the comparison between the present CFD results and the developed correlation (Equation 12) for two nozzle fluid temperatures and the matching seems to be very reasonable. As the louvers opening area increases the funnel sucks more ambient fluid into it. Thus, the low-temperature ambient fluid mixes with the hot plume in the funnel and the funnel exit temperatures falls as a result, which can be seen from Figure 12. When the louvers area still increases the mass suction into the funnel does not increase significantly so the funnel exit temperature remains constant.

A view of mass ingress into the funnel

Through the louvers on the funnel wall, outside air gets sucked into the funnel due to the creation of suction in the funnel (see Figures 8 and 9). A visual effect of suction into the funnel has been shown in Figure 13. From the outer boundary of the computational domain fine dust particles (no mass and insignificant diameter) were released. The particles get sucked into the funnel through the louvers and this can be seen clearly from Figure 13 which is a CFD representation of path lines of particles. The particles enter the louvers and rise up along with the main jet. The particles get sucked from the outer boundary of the domain as well as from the top of the domain because the top of the domain also feels the suction.

DOI: 10.1002/fld

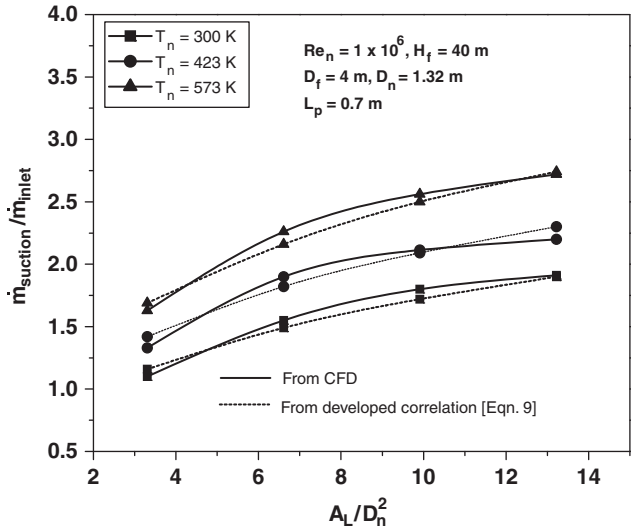

Figure 11. Ratio of rate of mass suction to the rate of inlet mass flow as a function of louvers opening area at nozzle fluid temperature: A comparison with the developed correlation.

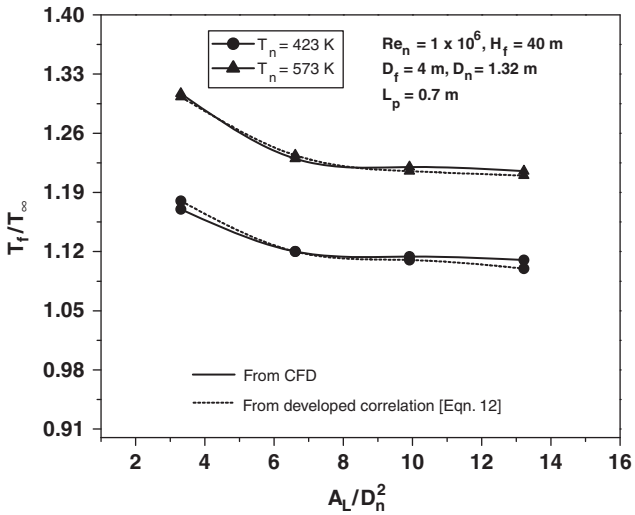

Figure 12. Funnel outlet temperature as a function of louvers opening area: A comparison with the developed correlation.

Effect of L_p/D_n on ratio of rate of mass ingress to the rate of mass injected from the nozzle

The effect of protruding length of the nozzle into the funnel on mass suction rate has been shown in Figure 14. It seems from the figure that the protruding length of the nozzle has no effect on the mass suction rate into the funnel. Actually for such tall funnel the effect of protruding length is almost nothing. But for a short funnel there exists an optimum protruding length where mass

DOI: 10.1002/fld

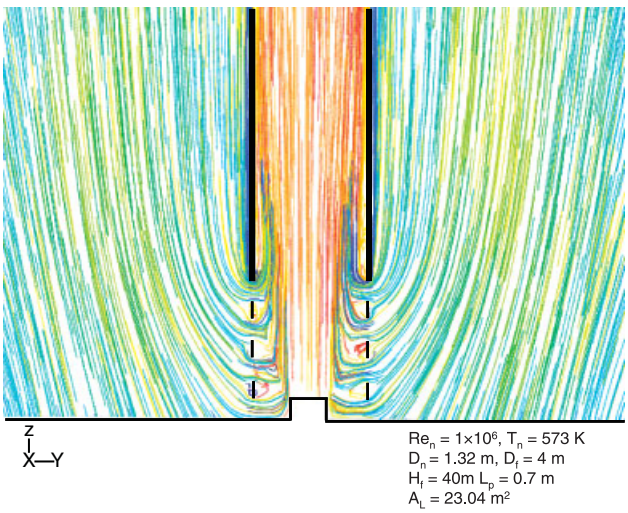

Figure 13. Expanded view of the path lines (y–z plane) around the louvers of the funnel, showing mass ingress into the funnel due to the drag/viscous effect produced by the main jet on the surrounding fluid.

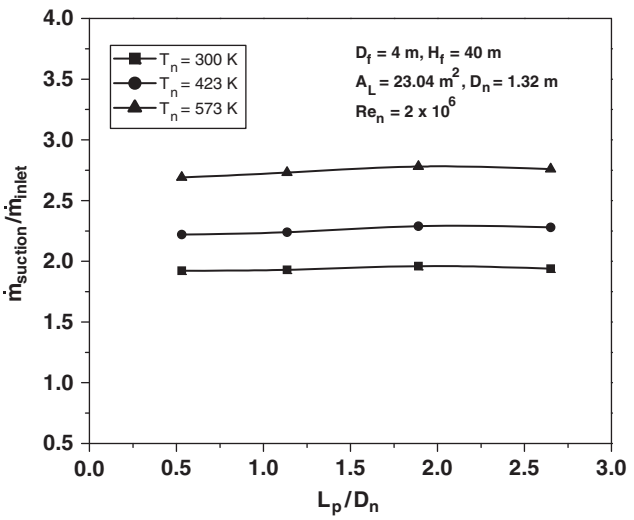

Figure 14. Ratio of rate of mass suction to the rate of inlet mass flow as a function of $L_{\mathrm{p}}/D_{\mathrm{n}}$ at different temperatures.

suction into the funnel is again highest. If the funnel is short then the louvers are placed close to each other and the protruding length of the nozzle can create a different pressure field inside the funnel for which the mass suction can be different. But for a tall funnel even if the nozzle protrudes much more into the funnel it can create a pressure field which will even disturb the suction from the first row of louvers. Therefore, the effect of $L_{\mathrm{p}}/D_{\mathrm{n}}$ on mass suction will be almost nothing for a tall funnel.

DOI: 10.1002/fld

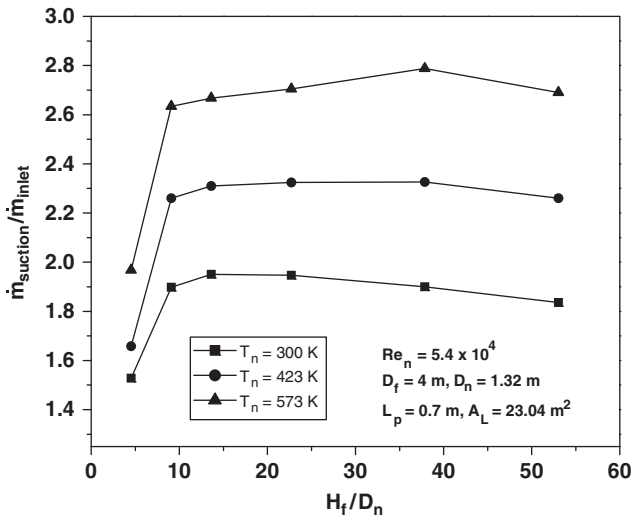

Figure 15. Variation of ratio rate of suction to the rate of inlet mass flow as a function of H_f/D_n and nozzle fluid temperature.

Effect of H_f/D_n on mass ingress

The effect of H_f/D_n on mass suction rate into the funnel is shown in Figure 15. It is clear from Figure 15 that there exists an optimum funnel height for highest mass suction to occur. For the particular case shown in Figure 15 the optimum height is 40 m. The mass suction into the funnel suddenly jumps from a low value to a high value as the value of H_f/D_n changes from 5 to 10. This means that for a short funnel the mass suction is low for a particular nozzle mass injection and as the funnel becomes taller and taller and the mass suction increases for the same nozzle mass injection. If the funnel is short then the (funnel top pressure is atmospheric) pressure distribution in the funnel due to mass injection can be very much different from that of a tall funnel which can cause the mass suction to be very much different. As is seen from Figure 15, when H_f/D_n increases beyond 10 the mass suction rate in the funnel rises very slowly and attains a peak at 40 and thereafter it falls a bit signifying that $H_f/D_n = 40$ is the optimum funnel height for highest mass suction rate. If the funnel is too tall then it offers again high viscous resistance to the flow for which the mass suction into it falls after a certain value of H_f/D_n.

Entrance length for a sucking pipe or cylindrical funnel

The funnel sucks air from the atmosphere and as a result has lot more turbulent mixing in it just after the louvers are over. From there onwards the flow tries to attain a developed state. It attains the state very quickly compared with a similar case of simple pipe at same Re where there is no suction (because the entrance condition for a sucking pipe is too different from that of a simple pipe without suction). It is to be noted that $L_e/D_f = 4.4Re^{1/6}$ for a simple pipe which is much larger compared with the sucking pipe. Figure 16 shows the entrance length as a function of D_f/D_n and in it the correlation developed from 228 data points of CFD run has been written. From Figure 16 it can be seen that there exists an optimum ratio of funnel to nozzle diameter where the entrance

DOI: 10.1002/fld

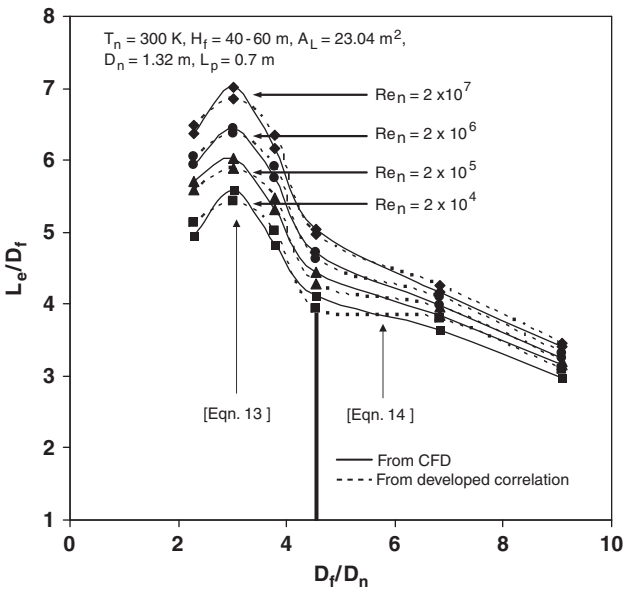

Figure 16. Variation of L_e/D_f as a function of D_f/D_n and Re_n: A comparison with the developed correlation.

length is highest. Of course the entrance length is of no consequence in deciding the mass suction, but comes as a bi-product of the present study which can be of academic interest and value. The ratio of L_e/D_f will always have a peak when plotted against D_f/D_n (for a sucking pipe only) which is shown in Figure 16. Figure 16 also shows a comparison of the CFD result with that of the developed correlation which are shown in Equations (13) and (14)

$$\frac{L_e}{D_f}=(2.763+0.1682\ln(Re_n))\left(\frac{A_L}{D_n^2}\right)^{0.0162}\left(0.035+0.768\frac{D_f}{D_n}-0.1295\left(\frac{D_f}{D_n}\right)^2\right)\left(\frac{T_n}{T_\infty}\right)^{0.1327} \quad (13)$$

$$\frac{L_e}{D_f}=(1.048+0.02147\ln(Re_n))\left(\frac{A_L}{D_n^2}\right)^{0.112}\left(3.573-0.1882\frac{D_f}{D_n}\right)\left(\frac{T_n}{T_\infty}\right)^{0.0715} \quad (14)$$

Equation (13) predicts at the worst an error of 10% only for two points at low Re and the rest 108 points are limited to an error of 8%. Equation (14) also predicts at the worst an error of 10% for only two points and the rest 116 data points are limited to an error of 7%. The L_e/D_f correlation has to be developed separately for two different regions of D_f/D_n just to keep the relatives error below 10%.

CONCLUSIONS

Numerical solution of the conservation equations for mass, momentum and energy along with the turbulent quantities for a funnel flow could be done to predict the mass flow rate into the funnel

DOI: 10.1002/fld

and the entrance length that would develop in the funnel in terms of the non-dimensional quantities as has been shown in Equations (13) and (14) and these correlations could predict the actual CFD result to a very good accuracy (the worst case is only 10% for two data points). The entrance length for a sucking pipe is found to be much lower compared with a simple pipe having the same Reynolds number. The developed correlation for mass suction, exhaust plume temperature and entrance length will be very useful to the funnel designers of ships. From the study it can also be concluded that there exists optimum $D_f/D_n = 4.55$ and $H_f/D_n = 40$ where the mass suction into the funnel can be the highest. The parameter D_f/D_n has the highest effect on mass suction rate into the funnel, a change of D_f/D_n from 2.2 to 4.55 can change the mass suction rate by 130% at a temperature of 573 K. Then the parameter A_L/D_n^2 has the second highest effect on mass suction rate. A change of A_L/D_n^2 from 2.2 to 13 can change the mass suction rate by 90%.

APPENDIX A: UNCERTAINTY ANALYSIS

The entrainment rate $\dot{m}_{suc} = f(\rho, v, r, Q_{in})$.

Let W_m be the uncertainty in the result and w_ρ, w_v, w_r and w_Q be the uncertainties in the independent variable due to density of the air, velocity, radial distance and inlet volume flow rate. Then the uncertainty in the result due to these odds is given by Holman [7]

$$W_m = \left[\left(\frac{\partial \dot{m}_{suc}}{\partial \rho} w_\rho \right)^2 + \left(\frac{\partial \dot{m}_{suc}}{\partial v} w_v \right)^2 + \left(\frac{\partial \dot{m}_{suc}}{\partial r} w_r \right)^2 + \left(\frac{\partial \dot{m}_{suc}}{\partial Q_{in}} w_Q \right)^2 \right]^{1/2}$$

$$\dot{m}_{suc} = \dot{m}_{tot} - \dot{m}_{in} = \rho(\pi r^2 v - Q_{in})$$

For a particular case $\dot{m}_{in} = 1.2 \times 10^{-3}\,\text{kg/s} \Rightarrow Q_{in} = 1 \times 10^{-3}\,\text{m}^3/\text{s}$, assuming $\rho = 1.2\,\text{kg/m}^3$ at 20°C and $\dot{m}_{tot} = 7.11 \times 10^{-3}\,\text{kg/s}$.

For a 0.07 m radius funnel the average velocity, $v = 0.385\,\text{m/s}$.

Here uncertainty of individual parameter is specified as,

Density, $\rho = 1.2 \pm 0.00237\,\text{kg/m}^3$ (though we are not measuring the density but it is expected to vary within that range at room temperature and pressure).

The error in the room temperature measurement is 0.2°C in 20°C which gives rise to 0.068% relative error in temperature. The error in laboratory pressure is 1 mm in 760 mm of Hg which gives rise to 0.13% relative error in pressure. The net error in density will be 0.198% which is $0.00237\,\text{kg/m}^3$.

Radius, $r = 0.07 \pm 0.0005\,\text{m}$.

Velocity, $v = 0.385 \pm 0.00577\,\text{m/s}$ (1.5% specified by the anemometer manufacturer).

Volume flow rate, $Q_{in} = (1 \pm 0.03) \times 10^{-3}\,\text{m}^3/\text{s}$ (3% specified by the rotameter manufacturer).

Nominal value of the entrainment rate, $\dot{m}_{suc} = \rho(\pi r^2 v - Q_{in}) = 5.91 \times 10^{-3}\,\text{kg/s}$

$$\frac{\partial \dot{m}_{suc}}{\partial \rho} = \pi r^2 v - Q_{in} = 4.926 \times 10^{-3}$$

$$\frac{\partial \dot{m}_{suc}}{\partial v} = \rho \pi r^2 = 0.0184$$

DOI: 10.1002/fld

$$\frac{\partial \dot{m}_{\text{suc}}}{\partial r} = 2\pi r \rho v = 0.2032$$

$$\frac{\partial \dot{m}_{\text{suc}}}{\partial Q_{\text{in}}} = -\rho = -1.2$$

Thus, the uncertainty in the entrainment rate is

$$\begin{aligned} W_m &= [(4.926 \times 10^{-3} \times 0.00237)^2 + (0.0184 \times 0.00577)^2 \\ &\quad + (0.2032 \times 0.0005)^2 + (-1.2 \times 0.03 \times 10^{-3})^2]^{1/2} \\ &= 1.517 \times 10^{-4}\,\text{kg/s} \end{aligned}$$

or

$$\frac{W_m}{\dot{m}_{\text{suc}}} = \frac{1.517 \times 10^{-4}}{5.91 \times 10^{-3}} = 0.02567 = 2.567\%$$

NOMENCLATURE

A_{L}	louvers opening area
D_{cd}	diameter of computational domain
D_{f}	diameter of the funnel
D_{n}	nozzle diameter
$\mathbf{g}$	acceleration due to gravity
G_k	production of turbulent kinetic energy
H_{cd}	height of the computational domain
H_{f}	height of the funnel
k	turbulent kinetic energy
L_{p}	protruding length of nozzle
L_{e}	entrance length
$\dot{m}_{\text{inlet}}$	mass flow rate through the nozzle
$\dot{m}_{\text{suction}}$	air suction rate through the louvers
p	pressure
Pr	v/α
Pr_t	turbulent Prandtl number
Q_{inlet}	volume flow rate through the nozzle
Q_{suction}	volumetric air suction rate
Re_{n}	$\rho V_{\text{n}} D_{\text{n}}/\mu$
T	temperature
$\mathbf{v}$	velocity vector
V_{n}	outlet velocity at nozzle exit

DOI: 10.1002/fld

Greek symbols

ρ	density
μ	shear viscosity
μ_t	turbulent viscosity
μ^{eff}	effective viscosity
$\overline{\overline{\tau}}$	stress tensor
ε	rate of dissipation
σ_k	turbulent Prandtl number for k
σ_ε	turbulent Prandtl number for ε

Subscripts

n	nozzle
∞	free stream
f	exit fluid

REFERENCES

1. Dash SK. Heatline visualization in turbulent flow. *International Journal of Numerical Methods for Heat and Fluid Flow* 1996; **6**(4):37.
2. Jha PK, Dash SK. Effect of outlet positions and various turbulence models on mixing in a single and multi strand tundish. *International Journal of Numerical Method for Heat and Fluid Flow* 2002; **12**(5):560–584.
3. Jha PK, Dash SK. Employment of different turbulence models to the design of optimum steel flows in a tundish. *International Journal of Numerical Methods for Heat and Fluid Flow* 2004; **14**(8):953–979.
4. Jha PK, Rajeev R, Mondal SS, Dash SK. Mixing in a tundish and a choice of turbulence model for its prediction. *International Journal of Numerical Methods for Heat and Fluid Flow* 2003; **13**(8):964–996.
5. Singh GS, Sundararajan T, Bhaskaran KA. Mixing and entrainment characteristics of circular and noncircular confined Jets. *Journal of Fluid Engineering*, *ASME* 2003; **125**:835–842.
6. Prichard R, Guy JJ, Conner NE. *Industrial Gas Utilization*. Bowker: New Providence, NJ, 1977.
7. Holman JP. *Experimental Methods for Engineers* (6th edn). McGraw-Hill International: New York, 1994; 49.

DOI: 10.1002/fld